Brazilian Journal of Medical and Biological Research (2004) 37: 929-935
ISSN 0100-879X

Ca_V 3.1 and Ca_V 3.3 account for T-type Ca^{2+} current in GH3 cells

M.A. Mudado[1], A.L. Rodrigues[1], V.F. Prado[2], P.S.L. Beirão[1] and J.S. Cruz[1]

Laboratórios de [1]Membranas Excitáveis and [2]Neurobiologia Molecular, Departamento de Bioquímica e Imunologia, Instituto de Ciências Biológicas, Universidade Federal de Minas Gerais, Belo Horizonte, MG, Brasil

Abstract

T-type Ca^{2+} channels are important for cell signaling by a variety of cells. We report here the electrophysiological and molecular characteristics of the whole-cell Ca^{2+} current in GH3 clonal pituitary cells. The current inactivation at 0 mV was described by a single exponential function with a time constant of 18.32 ± 1.87 ms (N = 16). The I-V relationship measured with Ca^{2+} as a charge carrier was shifted to the left when we applied a conditioning pre-pulse of up to -120 mV, indicating that a low voltage-activated current may be present in GH3 cells. Transient currents were first activated at -50 mV and peaked around -20 mV. The half-maximal voltage activation and the slope factors for the two conditions are -35.02 ± 2.4 and 6.7 ± 0.3 mV (pre-pulse of -120 mV, N = 15), and -27.0 ± 0.97 and 7.5 ± 0.7 mV (pre-pulse of -40 mV, N = 9). The 8-mV shift in the activation mid-point was statistically significant ($P < 0.05$). The tail currents decayed bi-exponentially suggesting two different T-type Ca^{2+} channel populations. RT-PCR revealed the presence of α1G (CaV3.1) and α1I (CaV3.3) T-type Ca^{2+} channel mRNA transcripts.

Correspondence
J.S. Cruz
Departamento de Bioquímica e Imunologia, ICB, UFMG
31270-901 Belo Horizonte, MG
Brasil
Fax: +55-31-3441-5963
E-mail: jcruz@icb.ufmg.br

Research supported by CNPq, CAPES and TWAS. J.S. Cruz, V.F. Prado and P.S.L. Beirão are recipients of CNPq research fellowships.

Received June 2, 2003
Accepted February 26, 2004

Key words
- Calcium channel
- T-type
- Electrophysiology
- RT-PCR
- GH3 cells

Introduction

The entry of calcium into cells through voltage-gated Ca^{2+} channels is responsible for a number of intracellular signaling events. Molecular cloning studies have characterized at least 10 genes encoding six different Ca^{2+} channels (1). Much of the effort devoted to gathering information to elucidate their mechanisms of action is based on the use of heterologous expression systems to avoid contaminating currents. The T-type Ca^{2+} channel subfamily consists of three genes called α1G, α1H, and α1I (2,3). Many reports have characterized both the biophysical and pharmacological features of each member of this subfamily (4-7).

GH3 cells are clonal somatomammotropic cells that have been used to study the mechanisms underlying prolactin and growth hormone secretion. As is the case for other pituitary cells, hormone secretion by GH3 cells is regulated by free intracellular Ca^{2+} concentration, which is controlled by Ca^{2+} influx through voltage-dependent Ca^{2+} channels. Under normal conditions, two types of Ca^{2+} currents can be demonstrated in GH3 cells: L-type, high voltage-activated and T-type, low voltage-activated Ca^{2+} currents (8). Whereas L-type Ca^{2+} channels have been

extensively studied, the absence of a pharmacological agent specific for T-type Ca^{2+} channels has hampered the study of their physiological role. As a consequence, few reports are available concerning T-type Ca^{2+} currents in GH3 cells. In a recent paper (9) the functional expression of T-type Ca^{2+} channels in one sub-clonal line (GH3/B6) related to GH3 cells was reported. These investigators were able to isolate a very small and infrequent (~10% of the cells) Ca^{2+} current, which they considered to be similar to T-type Ca^{2+} currents. They also reported the presence of only an α1G transcript. These two cell lines differ in some aspects, with GH3/B6 expressing more prolactin than GH3 cells. The molecular basis for the differences between these pituitary cell lines has not been determined. We then asked the following questions: What is the profile of T-type Ca^{2+} channel expression for GH3 cells? Can we measure T-type Ca^{2+} currents reliably? In order to answer these questions we used electrophysiological and RT-PCR techniques to characterize the T-type channel α1 subunits in neuroendocrine GH3 cells.

Material and Methods

RNA extraction and RT-PCR

Total RNA was extracted from GH3 cells using TRIZOL (Gibco BRL, Gaithersburg, MD, USA) according to manufacturer's instructions, and treated with deoxyribonuclease I (Gibco BRL). RT-PCR was carried out using the access RT-PCR introductory kit from Promega (Madison, WI, USA). The primers used (10) were α1G (5' CAG GAG ACG AAA CCT TGA 3' and 5' GAC GAG GAT AAG ACG TCT 3'), α1I (5' CAG GAT CCG GAA CTT GTT 3' and 5' GAT GAG GAC CAG AGC TCA 3'), and ß-actin (5' GTT CCG ATG CCC CGA GGA TCT 3' and 5' GCA TTT GCG GTG CAC GAT GGA 3'). Each tube contained 10 µl avian myeloblastosis virus (AMV)/Tfl 5X buffer, 10 mM dNTP, 25 µM each primer, 0.1 u/µl AMV reverse transcriptase (RT), 0.1 u/µl Tfl DNA polymerase, 0.15 µg/µl DNA-free RNA, and 29 µl nucleotide-free water to a final volume of 50 µl. Tubes were warmed to 48ºC for 45 min to allow reverse transcription and immediately submitted to amplification steps consisting of 2 min of denaturation at 94ºC followed by 40 cycles (30 s at 94ºC, 1 min at 55ºC, 2 min at 65ºC). PCR products were analyzed in a 0.8% agarose gel stained with ethidium bromide. For some unknown reason, primer used to visualize the α1H (CaV3.2) isoform did not work properly and we could not determine with certainty if GH3 cells expressed or not the CaV3.2 T-type Ca^{2+} channels.

Cell culture and electrophysiology

GH3 cells acquired from ATCC (Rockville, MD, USA) were cultured and maintained as described elsewhere (11,12). The standard pipette solution contained 100 mM CsCl, 10 mM EGTA, 2 mM $MgCl_2$, and 40 mM HEPES, pH adjusted to 7.2 with CsOH. In some experiments we used fluoride-rich internal solutions that contained 80 mM CsF, 20 mM CsCl, 2 mM $MgCl_2$, 10 mM EGTA, and 40 mM HEPES, pH 7.2 with CsOH to accelerate the run-down of high voltage-activated Ca^{2+} currents (13). The external solution contained 130 mM CsCl, 5 mM $CaCl_2$, 0.5 mM $MgCl_2$, 10 mM HEPES, and 5 mM glucose, pH adjusted to 7.4 with CsOH. In some experiments we used 10 µM nicardipine to block the L-type Ca^{2+} current but unfortunately we found that this concentration also inhibited the T-type Ca^{2+} current. Thereafter, we did not use nicardipine. All experiments were carried out at room temperature (22-25º). To analyze the voltage dependence for activation a modified Boltzmann equation was used to fit the experimental points:

$$I/I_{max} = (1 + A)/\{1 + \exp[(V_{1/2} - V_m)/k]\} + C,$$

where I is the current amplitude, I_{max} is the maximal current, $V_{1/2}$ is the activation midpoint, V_m is the membrane voltage, k is the slope factor, and A and C are the offsets. Inactivation and deactivation kinetics were fitted to single or double exponentials.

An EPC-9 patch-clamp amplifier and pulse software were used to measure whole-cell Ca^{2+} currents. Capacitive currents were compensated electronically and a P/4 protocol (14) was used for linear leak and residual capacitance subtraction. Ca^{2+} currents were low pass filtered at 2.5 kHz and sampled at 10 or 25 kHz. Pipettes were pulled from glass capillaries (Perfecta, São Paulo, SP, Brazil) and had resistances of 2-4 MΩ when filled with pipette solution. The holding potential used to measure I_{Ca} was -80 mV and a pre-pulse to -120 mV for 500 ms was applied immediately prior to the test pulses unless otherwise described. Cell membrane capacitances, used to normalize current amplitudes and thus minimize variance caused by differences in cell size, were measured automatically using a built-in routine in the Pulse software. Series resistance was compensated by 30 to 60%. Patch-clamp experiments were performed on 35-mm Petri dishes using an inverted microscope (Olympus, New Hide Park, NY, USA) with a 40X phase contrast objective. The bath was perfused continuously at 1-2 ml/min throughout the experiment. Solutions were gravity fed to the input ports of a solenoid valve mounted close to the bath, which was used to choose between one of two solutions. Further data were processed with Excel (Microsoft, Redmond, WA, USA) and SigmaPlot (SPSS Inc., Chicago, IL, USA).

Data are reported as means ± SEM and were analyzed statistically by the Student *t*-test, with the level of significance set at $P < 0.05$. Exponential fits were calculated by the method of Levenberg-Marquardt. The F-test for comparing two models such as single or double exponential fits was used.

Results

The whole-cell Ca^{2+} currents displayed in Figure 1 were evoked by a pair of 120-ms square pulses to 0 mV, with a 10-ms interval to assure that T-type channels would not fully recover from inactivation. A rapidly decaying inward current followed by a sustained component was recorded in response to the first pulse (see Figure 1A). Since T-type Ca^{2+} channels recover from inactivation slowly (~300 ms is a typical value; 1) the second Ca^{2+} current elicited in response to a step depolarization after the 10-ms interval at -80 mV showed only the sustained component. The digital subtraction of the second current record from the first revealed a fast inactivating inward Ca^{2+} current (Figure 1B). The current inactivation at 0 mV was described by a single exponential function with a time constant of 18.32 ± 1.87 ms (N = 16).

Figure 2A shows a family of current traces recorded in response to a voltage-clamp protocol. A conditioning step to -120 mV was applied for 500 ms to recruit T-type Ca^{2+} channels from inactivation, and then the voltage was increased to various membrane potentials from -60 to -10 mV. When the cell was depolarized to potentials more positive than -60 mV a transient inward current appeared at the onset of the test pulse followed by a sustained component that showed very slow decay.

Figure 2B illustrates sample current recordings elicited by voltage steps from -50 to -10 mV. Importantly, a 500-ms conditioning

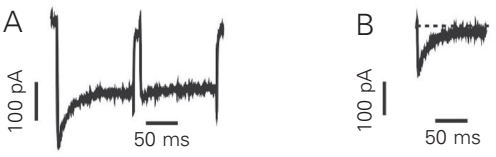

Figure 1. Whole-cell inward Ca^{2+} currents evoked by a double-pulse protocol in GH3 neuroendocrine cells. *A,* Representative traces in response to step depolarization to 0 mV for 120 ms from a holding potential of -80 mV. The first current trace corresponds to the activation of both T-type (transient) and L-type Ca^{2+} (sustained) currents. The second trace was recorded after a brief time at -80 mV (10 ms) and then a return to 0 mV. The recorded current trace represents only L-type Ca^{2+} current (sustained) because T-type channels were inactivated. *B,* Current trace obtained by digitally subtracting the current evoked after the pre-pulse from that before the pre-pulse as in *A.*

pulse to -40 mV was applied to inactivate T-type Ca^{2+} channels. All recorded currents decayed more slowly. Figure 2C and D shows the peak current normalized by the cell capacitance and plotted as a function of membrane voltage. Composite data indicate that the current density obtained from -120 mV (Figure 2C) was higher than that obtained by subtracting current traces between the two different holding potentials (Figure 2D, open circles). The continuous line (Figure 2D) represents the I-V relationship as plotted in Figure 2C. As indicated, the difference-Ca^{2+} current began to appear at -60 mV and peaked at about -30 mV (Figure 2D, open circles). Our results revealed the presence of a low voltage-activated Ca^{2+} current in GH3 cells which is consistent with reported data (13).

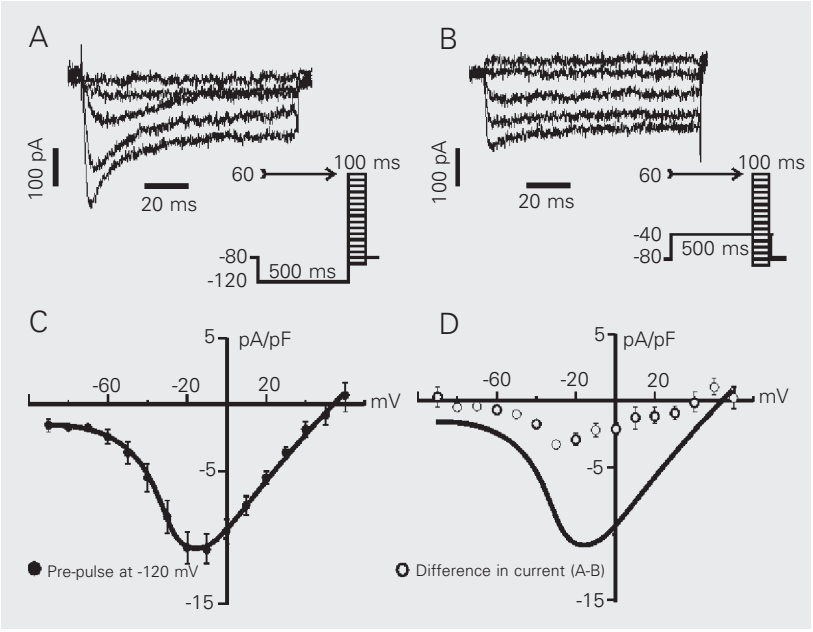

Figure 2. Current-voltage relationships (I-V) in GH3 cells. *A*, Current traces evoked by depolarizations from -60 mV to -20 mV (holding potential -80 mV, pre-pulse -120 mV). *B*, Current traces elicited by depolarizations from -50 mV to -10 mV (holding potential -80 mV, pre-pulse -40 mV). *C*, Averaged density current-voltage relationship obtained for GH3 Ca^{2+} currents (filled circles, N = 15). Currents were normalized to cell capacitance to avoid variability due to cell size. *D*, Averaged current density-voltage relationships for peak currents obtained using a pre-pulse at -120 mV (continuous line), and after subtracting current traces between the two different holding potentials (Figure 2D, open circles, N = 7). All recordings were done using 5 mM calcium as the charge carrier. Data in *panels C* and *D* are reported as means ± SEM.

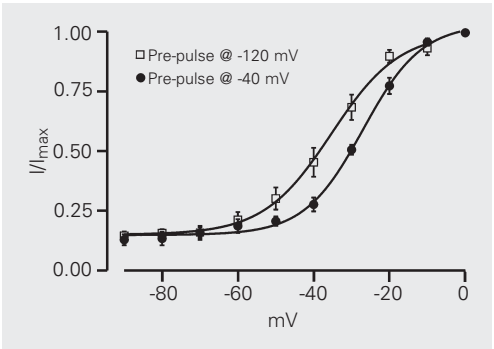

Figure 3. Voltage-dependent activation of GH3 Ca^{2+} currents. The peak current at each potential was normalized to the maximum peak current and was averaged for each potential. The symbols indicate composite data obtained from a pre-pulse set at -120 mV (squares, N = 15) and from a pre-pulse at -40 mV (circles, N = 9). Solid lines represent the fitting of Boltzmann equations with half-activation voltages of -35.02 mV (pre-pulse at -120 mV) and -27.04 mV (pre-pulse at -40 mV) and slope factors of 6.65 (pre-pulse at -120 mV) and 7.51 (pre-pulse at -40 mV).

To characterize the activation properties we generated normalized current-voltage curves (Figure 3). The half-maximal voltage activation ($V_{1/2}$) and the slope factors (k) for the two conditions are -35.02 ± 2.4 and 6.7 ± 0.3 mV (Figure 3, pre-pulse of -120 mV, squares, N = 15), and -27.0 ± 0.97 and 7.5 ± 0.7 mV (Figure 3, pre-pulse of -40 mV, circles, N = 9). The 8-mV shift in the activation mid-point was statistically significant ($P < 0.05$).

A distinguishing feature of native T-type Ca^{2+} channels is their slow deactivation kinetics (1). The rate of deactivation was measured as the rate of decay of the tail currents at different repolarizing membrane potentials (Figure 4 and Table 1). Somewhat surprisingly, the tail currents were best fitted by a double exponential, an unexpected finding since deactivation kinetics described for T-type Ca^{2+} current should follow a mono-exponential decay (10). However, there are recent reports suggesting that CaV3.3 (α1I) channels close in a biexponential manner (15-17). It has been well established that GH3 cells contain two types of voltage-dependent Ca^{2+} channels (L- and T-type channels) (8,18). The voltage dependence of deactivation was examined in a potential range (-120 to -60 mV) to avoid any interference by L-type Ca^{2+} channels (18). It is possible that the protocol used to measure tail currents was revealing L-type Ca^{2+} channel deactivation along with T-type deactivation. This could account, at least in part, for the fast component of the tail currents. Another

explanation is that GH3 cells express more than one T-type Ca^{2+} channel and, as suggested above, the CaV3.3 (α1I) channel actually deactivates faster than the other T-type channels (19). Prompted by a study describing the acceleration of L-type Ca^{2+} channels run-down by substituting fluoride for chloride in the pipette solution (13), we performed a similar analysis in which the L-type Ca^{2+} current was presumably abolished, allowing us to record a "pure" T-type Ca^{2+} current. Figure 4B shows a family of tail currents recorded from a GH3 cell. The tail current decay was well described by the sum of two exponentials (see also Table 1). The fitted time constants are shown in Figure 4D. Figure 5 illustrates the tail currents from Figure 4B on a faster time scale. Over the range of voltages at which channels deactivate significantly, the tail currents were better described by the sum of two exponentials (Figure 5B). Although only 30 ms is shown in Figure 5, the currents were fitted over the entire 100-ms pulse duration. To our surprise, the fast and slow time constants measured in fluoride-rich internal solution showed

Table 1. Summary of the parameters used to obtain the best fit for the deactivation kinetics.

Potential (mV)	c (pA)	A_1 (pA)	τ_1 (ms)	A_2 (pA)	τ_2 (ms)	R^2
-50	-46.85 ± 7.97	-189.3 ± 24.5	7.62 ± 1.01	-43.36 ± 13.69	1.23 ± 0.31	0.947
-60	-36.69 ± 4.69	-143.4 ± 31.5	7.68 ± 4.4	-139.67 ± 45.26	2.87 ± 0.41	0.957
-70	-25.02 ± 4.31	-166.4 ± 24.8	7.87 ± 1.81	-170.84 ± 32.04	1.76 ± 0.14	0.956
-80	-21.56 ± 2.32	-138.5 ± 58.3	8.02 ± 3.68	-250.77 ± 30.10	1.42 ± 0.21	0.960
-90	-25.13 ± 2.63	-120.7 ± 31.8	3.67 ± 0.83	-314.82 ± 54.27	1.03 ± 0.15	0.957
-100	-17.58 ± 4.33	-112.7 ± 24.7	3.3 ± 0.59	-350.70 ± 36.60	0.86 ± 0.05	0.944
-110	-22.67 ± 3.70	-108.3 ± 36.6	2.15 ± 0.49	-378.38 ± 28.19	0.704 ± 0.06	0.926
-120	-26.11 ± 3.98	-280.0 ± 35.9	6.14 ± 0.75	-454.77 ± 40.30	0.609 ± 0.02	0.925

Data are reported as means ± SEM. A_1 and A_2 are the amplitudes of slow and fast components, and τ_1 and τ_2 are the slow and fast time constants for the tail current decay, respectively. The number of cells used was 4. c = offset (time-independent component); R^2 = Coefficient of determination.

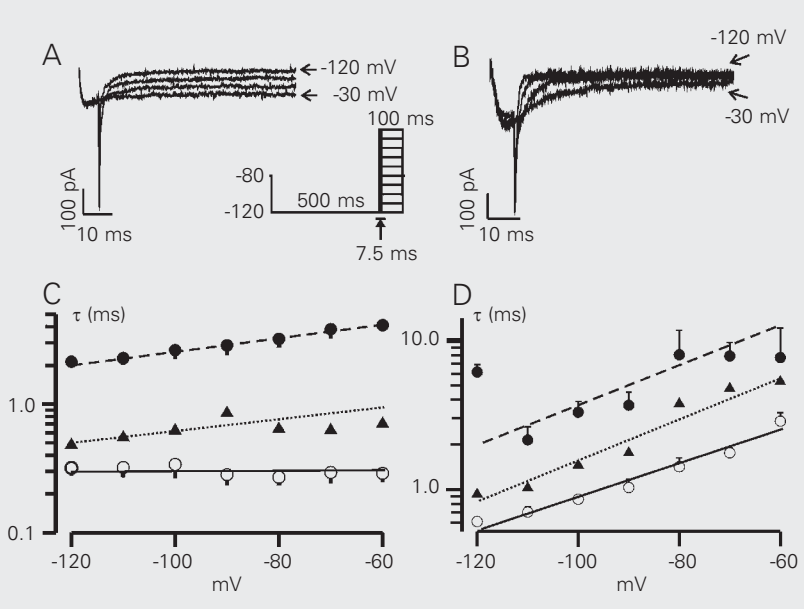

Figure 4. Voltage dependence of deactivation kinetics. *A*, Representative calcium current tail traces evoked by different repolarizing potentials between -120 and -30 mV. The pipette solution contained a high chloride concentration. *B*, Representative calcium tail currents. The voltage protocol was the same as in *A*. The pipette solution had a high concentration of fluoride ion. *C*, Plot of mean deactivation time constants (τ) against repolarization potentials. Data points are the two time constants, which represent the fast (open circles, N = 8) and slow components of the tail (filled circles, N = 8) current decay shown in *panel A*. Also shown is the weighted τ (τ_w, triangles) that was derived using the equation: $\tau_w = A_1\tau_{fast} + A_2\tau_{slow}$, where A_1 and A_2 are the normalized amplitudes of the fast and slow components. *D*, Deactivation time constants plotted as in *C*. The fast (open circles, N = 4) and slow (filled circles, N = 4) components are represented and were taken from current traces as shown in *panel B*. The triangles indicate the weighted time constant.

some differences when compared with those measured in chloride-rich internal solutions.

These findings are consistent with the idea of two isoforms being expressed in GH3 cells with different deactivation kinetics. An alternative view would be that the GH3 cells do express only one type of low voltage-activated channel, which deactivates bi-exponentially in a way similar to the CaV3.3 (α1I) channel.

As our time constants of deactivation were not sufficiently accurate to indicate which subunits are expressed in GH3 cells, we carried out an RT-PCR with primers specific for α1G (Figure 6, lanes 5 to 7) and α1I (Figure 6, lanes 8 to 10). The total extracted RNA was treated with DNAse to ensure that no genomic DNA was present when the reaction was performed. Lanes 5 and 8 show transcripts with molecular weights of ~800 bp and ~870 bp that are in agreement with previous sequencing data for the α1G and α1I subunits (10). We also used primers specific for ß-actin as a positive control (Figure 6, lanes 2 to 4).

The presence of transcripts for α1G and α1I is additional evidence that the GH3 cells are probably expressing these two functional subunits. This argument is supported by the presence of two distinct deactivation time constants for the Ca^{2+} currents when fluoride was used in the internal medium.

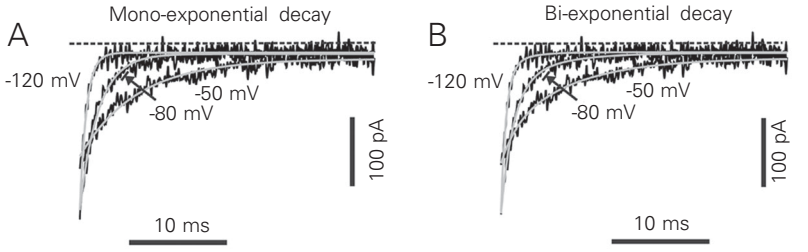

Figure 5. Exponential fits to tail currents. Records are from Figure 4B on an expanded time scale. The thicker smooth gray lines are fits to a single exponential (A, left) or the sum of two exponentials (B, right).

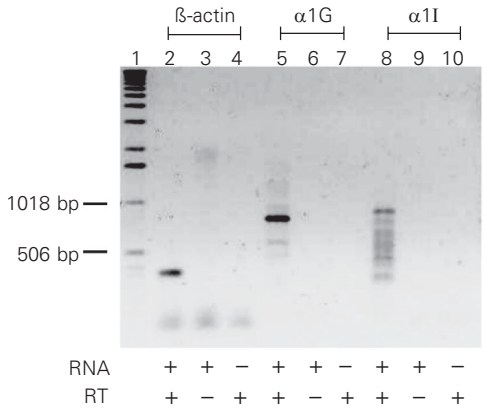

Figure 6. T-type Ca^{2+} channel subtypes in rat GH3 cells. RT-PCR performed to identify the presence of mRNA for the α1G and α1I subunits in GH3 cells. The positive control contained primers specific for ß-actin (lane 2). Negative controls did not include RNA or reverse transcriptase (RT) in the tubes (lanes 3, 4, 6, 7, 9 and 10).

Discussion

The use of GH3 as a model cell for testing drugs and toxins and for studying hormone secretion has been well established. The importance of knowing which types of channels are present in these cells is obvious since specific drugs can modulate channels in different ways.

In general, T-type Ca^{2+} channels display either similar or smaller peak currents upon replacement of Ca^{2+} with Ba^{2+} (20). Accordingly, in the present study we measured Ba^{2+} currents which were found to be identical to the currents measured when Ca^{2+} was used (data not shown). These results allow us to suggest that GH3 cells may not express the α1H isoform, which has been shown to conduct Ba^{2+} better than Ca^{2+} (10).

Close inspection of our I-V data (Figure 2C and D) shows that the 500-ms depolarizing pre-pulse to -40 mV seems not to prevent Ca^{2+} currents from being activated at relatively low membrane potentials (~-50 mV). As discussed above, this finding suggests the presence of low voltage-activated currents generated by L-type channels belonging to the α1D isotype. Since these channels deactivate faster than T-type channels we wondered if the time constants calculated using chloride-rich internal solutions (Figure 4C) were somehow faster than expected because of the contribution to the decay coming from deactivation of the α1D channels.

We examined the expression of T-type

Ca^{2+} channel subunits in GH3 cells to determine which subunits were present. Our results suggest that transient inward current flows in a combination of α1G and α1I channels. We used RT-PCR with primers specific for T-type Ca^{2+} channel subunit mRNA and obtained PCR products for α1G and α1I T-type Ca^{2+} channels (Figure 6). The presence of the α1G subunit in GH3 cells has been previously suggested (1) and is now confirmed by our data. In addition, we report the presence of the α1I subunit as a new finding.

In this report, we identified the molecular nature of T-type Ca^{2+} channels selectively expressed in the neuroendocrine GH3 cells. The combination of biophysical and molecular biological data led us to conclude that T-type Ca^{2+} currents in GH3 cells arise from α1G and α1I isoforms. Why do GH3 cells express two distinct T-type Ca^{2+} channels? Do they make different contributions to the electrical properties of GH3 cells? An exciting possibility is the implication of transient increases in $[Ca^{2+}]_i$ afforded by the differential expression profile of T-type Ca^{2+} channels in cell proliferation control.

References

1. Perez Reyes E (2003). Molecular physiology of low-voltage-activated T-type calcium channels. *Physiological Reviews*, 83: 117-161.
2. Huguenard JR (1998). Low-voltage-activated (T-type) calcium-channel genes identified. *Trends in Neurosciences*, 21: 451-452.
3. Perez Reyes E (1999). Three for T: molecular analysis of the low voltage-activated calcium channel family. *Cellular and Molecular Life Sciences*, 56: 660-669.
4. Berthier C, Monteil A, Lory P & Strube C (2002). Alpha(1H) mRNA in single skeletal muscle fibres accounts for T-type calcium current transient expression during fetal development in mice. *Journal of Physiology*, 539: 681-691.
5. Chemin J, Monteil A, Dubel S, Nargeot J & Lory P (2001). The alpha1I T-type calcium channel exhibits faster gating properties when overexpressed in neuroblastoma/glioma NG 108-15 cells. *European Journal of Neuroscience*, 14: 1678-1686.
6. Chemin J, Monteil A, Bourinet E, Nargeot J & Lory P (2001). Alternatively spliced alpha(1G) (Ca(V)3.1) intracellular loops promote specific T-type Ca($^{2+}$) channel gating properties. *Biophysical Journal*, 80: 1238-1250.
7. Todorovic SM, Perez-Reyes E & Lingle CJ (2000). Anticonvulsants but not general anesthetics have differential blocking effects on different T-type current variants. *Molecular Pharmacology*, 58: 98-108.
8. Armstrong CM & Matteson DR (1985). Two distinct populations of calcium channels in a clonal line of pituitary cells. *Science*, 227: 65-66.
9. Glassmeier G, Hauber M, Wulfsen I, Weinsberg F, Bauer CK & Schwarz JR (2001). Ca^{2+} channels in clonal rat pituitary cells (GH3/B6). *Pflügers Archiv*, 442: 577-587.
10. McRory JE, Santi CM, Hamming KS et al. (2001). Molecular and functional characterization of a family of rat brain T-type calcium channels. *Journal of Biological Chemistry*, 276: 3999-4011.
11. Kushmerick C, Kalapothakis E, Beirao PS et al. (1999). *Phoneutria nigriventer* toxin Tx3-1 blocks A-type K^+ currents controlling Ca^{2+} oscillation frequency in GH3 cells. *Journal of Neurochemistry*, 72: 1472-1481.
12. Leao RM, Cruz JS, Diniz CR, Cordeiro MN & Beirao PS (2000). Inhibition of neuronal high-voltage activated calcium channels by the omega-*Phoneutria nigriventer* Tx3-3 peptide toxin. *Neuropharmacology*, 39: 1756-1767.
13. Herrington J & Lingle CJ (1992). Kinetic and pharmacological properties of low voltage-activated Ca^{2+} current in rat clonal (GH_3) pituitary cells. *Journal of Neurophysiology*, 68: 213-233.
14. Bezanilla F & Armstrong CM (1977). Inactivation of the sodium channel. I. Sodium current experiments. *Journal of General Physiology*, 70: 549-566.
15. Frazier CJ, Serrano JR, George EG et al. (2001). Gating kinetics of the alpha1I T-type calcium channel. *Journal of General Physiology*, 118: 457-470.
16. Gomora JC, Murbartian J, Arias JM, Lee JH & Perez Reyes E (2002). Cloning and expression of the human T-type channel Ca(v)3.3: insights into prepulse facilitation. *Biophysical Journal*, 83: 229-241.
17. Murbartian J, Arias JM, Lee JH, Gomora JC & Perez Reyes E (2002). Alternative splicing of the rat Ca(v)3.3 T-type calcium channel gene produces variants with distinct functional properties(1). *FEBS Letters*, 528: 272-278.
18. Matteson DR & Armstrong CM (1986). Properties of two types of calcium channels in clonal pituitary cells. *Journal of General Physiology*, 87: 161-182.
19. Monteil A, Chemin J, Leuranguer V, Altier C, Mennessier G, Bourinet E, Lory P & Nargeot J (2000). Specific properties of T-type calcium channels generated by the human alpha 1I subunit. *Journal of Biological Chemistry*, 275: 16530-16535.
20. Hille B (2001). *Ion Channels of Excitable Membranes*. Sinauer Associates, Inc., Sunderland, MA, USA.